RESEARCH ARTICLE

A Wide-Scanning Metasurface Antenna Array for 5G Millimeter-Wave Communication Devices

GABRIELE FEDERICO[1,2], (Graduate Student Member, IEEE),
ANOUK HUBRECHSEN[1,3], (Graduate Student Member, IEEE),
SEBASTIAAN LAURENS COENEN[1,4], **AD C. F. RENIERS**[1,3],
DIEGO CARATELLI[1,2], (Senior Member, IEEE),
AND A. BART SMOLDERS[1,3], (Senior Member, IEEE)

[1]Department of Electrical Engineering, Eindhoven University of Technology, 5612 AZ Eindhoven, The Netherlands
[2]The Antenna Company, 5656 AE Eindhoven, The Netherlands
[3]Antennex B.V., 5612 AZ Eindhoven, The Netherlands
[4]Altum RF, 5612 AJ Eindhoven, The Netherlands

Corresponding author: Gabriele Federico (g.federico@tue.nl)

ABSTRACT In this paper we present a high-performance compact phased array antenna which is easy to integrate into mobile devices for 5G-and-beyond wireless telecommunications. The proposed design features high efficiency and wide-scan capabilities. The linear array consists of eight elements realized using substrate integrated waveguide technology in combination with two rows of metasurfaces that are used to optimize the transition towards free space for enhanced impedance matching characteristics. The integrated metasurface structure also enables a larger half-power beamwidth and wide-angle scanning at array level. A prototype has been realized using a dielectric substrate of Rogers RO4003C with relative permittivity of 3.55. The array is designed with an inter-element spacing of half-wavelength at 29.5 GHz and is characterized using dedicated millimeter-wave anechoic and reverberation chambers. The measurement results show that the proposed antenna array can scan from $\phi = -55°$ to $\phi = 55°$ with a gain fluctuation less than 3 dB in the frequency band of operation from 27 GHz to 29.5 GHz, and a measured total efficiency above 70 % with an uncertainty of 10% (95% confidence interval). Furthermore, when compared to the state-of-the-art, the proposed antenna provides a much wider scanning range while occupying a significantly smaller and compact volume.

INDEX TERMS 5G communications, beam forming, metasurfaces, phased array, wireless testing.

I. INTRODUCTION

With the advancement of new mobile communication technologies and the introduction of 5G networks, phased-array antennas operating at millimeter-wave (mm-wave) frequencies play a progressively more critical role in the successful deployment of such infrastructures. Enhanced gain characteristics at antenna system level are necessary to compensate for the propagation losses at high frequencies. Such performance can be achieved by integrating multiple radiating elements in an array configuration. The contradiction between the need for a large number of antenna elements being combined in the same system and the limited space typically available on printed circuit boards (PCBs) embedded in mobile devices makes the integration of multiple phased arrays challenging, though this is necessary to perform adaptive beamforming to guarantee full radio coverage.

In this context, one should notice that the integration of a large number of antenna elements in a limited portion of space poses problems in terms of power consumption and thermal management [1]. In this regard, an important role is played by the array beamforming network which could lead to extra insertion and radiation losses. Therefore, embedding the antenna array directly in the PCB of a 5G cellular device is useful to minimize the insertion loss between the antenna elements and the radio-frequency integrated circuits.

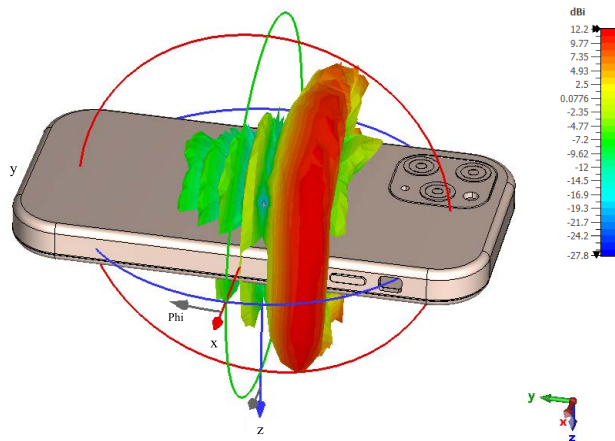The associate editor coordinating the review of this manuscript and approving it for publication was Giorgio Montisci.

FIGURE 1. Illustration of the 3D radiation pattern of the 1 × 8 antenna array which is contained in a smartphone housing.

Numerous papers are available in the scientific literature on different mm-wave antenna array technologies for integration in smartphones or mobile terminals [2]. Most of the proposed technical solutions rely on boresight-oriented patch antennas by virtue of the relevant ease of integration with the electronic components on the main PCB. Such antenna structures typically provide a maximum scan range up to ±50° [3].

In this work, we propose a compact end-fire like antenna array embedded in the PCB and realized using substrate integrated waveguide (SIW) technology. Such technology allows for easy integration and manufacturing in combination with mainstream PCB processes, and enables excellent radio frequency (RF) performance in terms of losses while preserving most of the advantages of traditional waveguides [4]. Antennas based on SIW technology represent sounding solutions for integration in PCBs with reduced available space. The main limitation is associated with the typical thickness of such PCBs which is much smaller than the height of traditional waveguide-based radiators. In combination with very thin dielectric substrates, having thicknesses typically below $\lambda_0/10$ (where λ_0 is the wavelength in free space), SIW-based open-ended waveguides usually have a very limited bandwidth [5]. For this reason, in this study, we propose the integration of metasurfaces to optimize the transition from the basic SIW structure to free space to improve the impedance matching characteristics of the antenna and increase the relevant bandwidth while enhancing the achievable realized gain [5]. At the same time, the adopted grid of metasurfaces is effective in enhancing the half-power beamwidth (HPBW) of the embedded antenna elements while reducing the parasitic coupling level between adjacent radiating elements. This is instrumental to the achievement of wide-scanning capabilities at array level.

The proposed 1 × 8 antenna array provides a typical end-fire like radiation pattern as illustrated in Fig. 1, and it is particularly suitable for mobile devices. Next to the array design concept, another original contribution of this research study is the use of a dedicated mm-wave reverberation chamber to accurately characterize, with a confidence level of
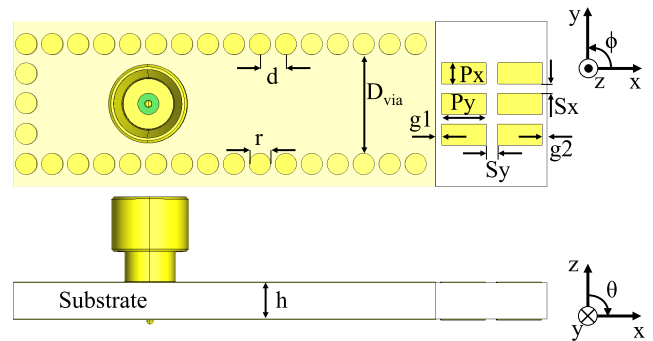

FIGURE 2. Top view and side view of the single element.

95 %, the realized antenna array efficiency [7]. As a matter of fact, one can notice that, in available scientific publications, the reported antenna efficiency levels at mm-wave frequencies are often based on numerical estimations only.

The paper is divided in three sections. In Section II, the geometry of the developed antenna element is presented. In Section III, the simulated array performance and the relevant measurement results are discussed. Finally, the concluding remarks are summarized in Section IV.

II. ANTENNA ARRAY GEOMETRY

The geometry of the proposed metasurface-based end-fire antenna is shown in Fig. 2. The bottom layer is hidden since it is identical to the top layer. Two rows of metal patches, on both the top and bottom metal layers, are integrated in such a way to optimize the impedance transition from the SIW-based open-ended waveguide structure to free space [8].

In the design of an open ended SIW, the main challenge is to match the characteristic impedance Z_s of the structure to the free-space impedance Z_{air}. Typically, $Z_{air} \simeq 377\Omega$ is much larger than Z_s. Therefore, strong reflections occur at the antenna aperture unless suitable design solutions are implemented.

The easiest way to improve impedance matching is to load the antenna with a dielectric material by extending the inner core of the substrate across the array aperture. In this way, the impedance level at the aperture can be modified by changing the realized effective permittivity ϵ_{eff}, as one can infer from the general relation between impedance and permittivity $Z = \sqrt{\mu_0/\epsilon_0\epsilon_{eff}}$, assuming that non-magnetic materials are being used.

In [9], the transition at array aperture is further improved by realizing perforations in the dielectric substrate. The diameter of such perforations increases with the distance from the aperture to synthesize smaller values of ϵ_{eff} and, thereby, a higher impedance. A more extensive review of end-fire antennas in SIW technology can be found in [10].

In this study, to enhance the impedance matching at the transition, we propose the integration of a suitable metasurface in combination with the basic SIW structure. Such a metasurface consists of metal patches printed on the extension of the substrate core at the array aperture (see
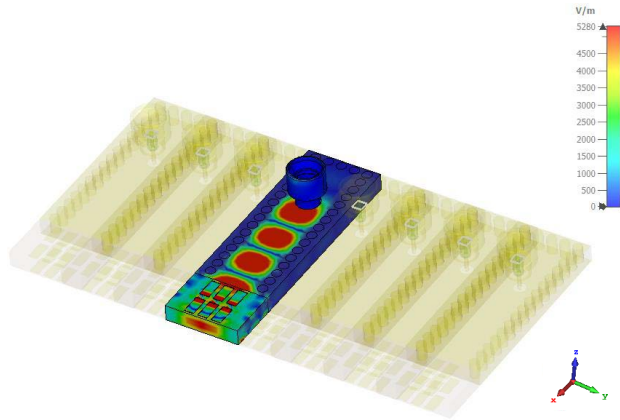
FIGURE 3. Metasurface antenna array where the TEM mode originating from the mini-SMP connector is transformed into the fundamental TE_{10} mode of the SIW.
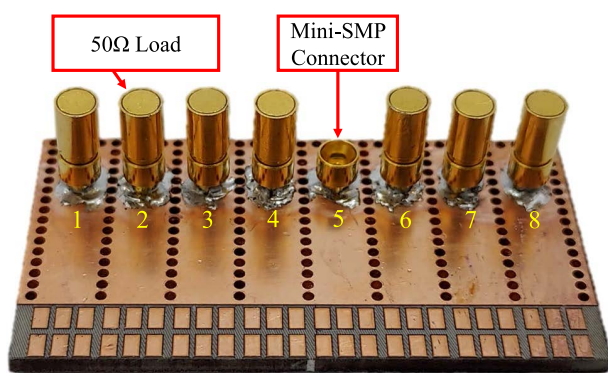

FIGURE 4. Manufactured antenna array with 50 Ω loads.

TABLE 1. Relevant dimensions of the proposed antenna element.

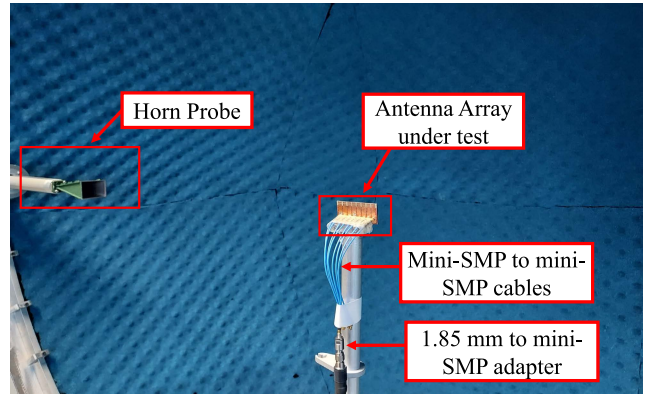| Parameter	Dimension (mm)	Parameter	Dimension (mm)
D_{via}	4.18	h	1.55
d	1.10	r	0.90
P_{x}	0.90	P_{y}	1.88
S_{x}	0.40	S_{y}	0.50
g_1	0.25	g_2	0.20

FIGURE 5. Gain pattern measurement setup of the linear array in a mm-wave anechoic chamber using a standard gain horn antenna [6].

Fig. 2). As shown in [11], the impedance of a substrate with double-sided parallel-strip lines, when neglecting the coupling between neighboring patches, can be calculated as:

$$Z_c = \frac{120\pi}{\sqrt{\epsilon_{\text{eff}}}\left[T + 1.393 + 0.667\ln(T + 1.444)\right]} \quad (1)$$

$$\epsilon_{\text{eff}} = \frac{\epsilon_r + 1}{2} + \frac{\epsilon_r - 1}{2}\frac{1}{\sqrt{1 + \frac{10}{T}}} \quad (2)$$

$$T = \frac{P_x}{h}, \qquad (P_x > h). \quad (3)$$

An approximate value of the patch length P_y can be derived as a function of the central working frequency f_r, using the following expression [8]:

$$P_y = \frac{2f_r\sqrt{\epsilon_r}}{c_0} - 0.7h \quad (4)$$

which properly accounts for the field fringing effects [12] and where c_0 is the speed of the light in free space.

More rows of metasurface elements can be used to make the transition to free space smoother. In literature, metasurfaces with multiple rows of elements are often adopted in such a way to enhance the antenna gain [13]. In our study, however, we make use of two rows only to mitigate the peak

gain of the individual array element while increasing the HPBW. Fig. 6 shows the normalized radiation pattern of the central antenna element embedded in the array structure with and without metasurfaces. One can notice that the integration of the metasurfaces significantly enhances (nearly doubling) the HPBW of the basic antenna element. At the same time, a considerable improvement is achieved in reducing the coupling with the adjacent elements, as shown in Fig. 6c, with a similar decoupling mechanism as shown in [14]. This, in turn, is useful to enable wide-angle scanning capabilities at array level.

The dimensions of the metal patches forming the metasurface can be tuned to control the impedance matching characteristics of the antenna and the center frequency of operation. The working principle of the considered metasurface is based on the observation that the current flow in the $y-$ direction, along the metal patches and across the relevant gaps, can be modeled, at circuit level, as a series of inductors and capacitors, respectively [5]. Therefore, the length of the metal patches and the gap between them have a tremendous impact on the achievable impedance matching characteristics of the antenna structure.

The proposed antenna element is fed by a mini-SMP connector type 18S101-5H0E4. The mini-SMP connector is only used for passive testing, but it is not required when the antennas are directly connected to beamforming integrated circuits (ICs). The feeding pin of the mini-SMP connector is inserted in an unplated via hole with a diameter equal to 0.4 mm, while the outer metal surface of the connector is soldered on top of the SIW structure. To prevent risk of short-circuiting, the
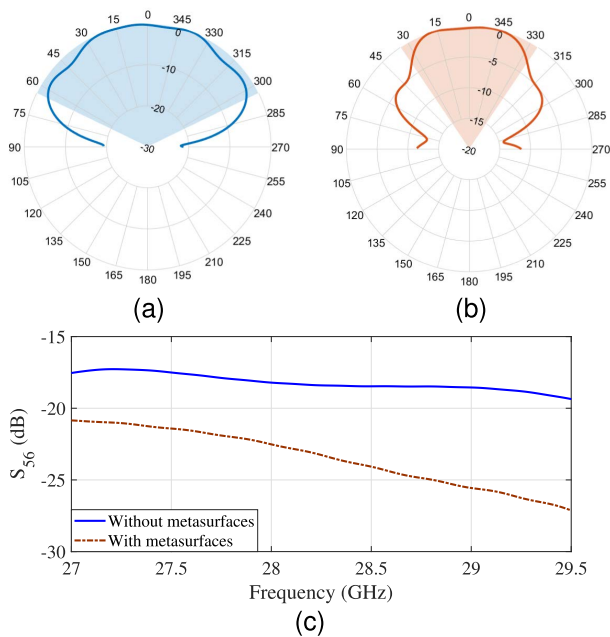
(a)

(b)

(c)

FIGURE 6. HPBW of the embedded element pattern (a) with and (b) without metasurfaces at 28 GHz, and (c) coupling level between the central array element and the adjacent element.

FIGURE 7. Efficiency measurement setup in a mm-wave reverberation chamber [7].

FIGURE 8. Measured and simulated S-parameters of the central and edge array elements.

bottom and top layers of the SIW include a circular clearance with a diameter of 1.1 mm around the feeding pin.

To determine the optimal dimensions of the metasurface for enhanced impedance matching, a dedicated parameter study has been carried out using CST Microwave Studio ©. Each antenna element has dimensions of 22.61 mm × 7 mm, and is printed on a Rogers RO4003C dielectric substrate with relative permittivity $\epsilon_r = 3.38$, loss tangent $\tan \delta = 0.0027$ (at 10 GHz), and thickness $t = 1.55$ mm. The relevant design parameters are summarized in Table 1. The simulation model of a 1×8 linear array based on the proposed antenna-element design is illustrated in Fig. 3 in combination with the electric field distribution originated by the incident TEM mode which propagates along the coaxial line and is transformed into the fundamental TE_{10} mode along the SIW. The complete array structure has dimensions of 41.53 mm × 22.60 mm, with the various antenna elements being separated by 5.08 mm (approximately $\lambda_0/2$ at 29.5 GHz). The manufactured 1×8 linear array demonstrator is shown in Fig. 4, where 7 of the 8 ports are terminated with 50 Ω loads.

III. SIMULATION AND MEASUREMENT RESULTS

The characterization of the array performance has been carried out with special focus on the radiation pattern and the radiation efficiency. The first parameter is to evaluate the beam-steering capability, whereas the latter provides a measure of loss occurring in the structure. An anechoic chamber is used for radiation pattern measurements, whereas, by means of a suitable reverberation chamber, the radiation efficiency of the antenna can be accurately evaluated to verify the simulated low-loss properties. As a matter of fact, a reverberation chamber is used because it can yield significantly
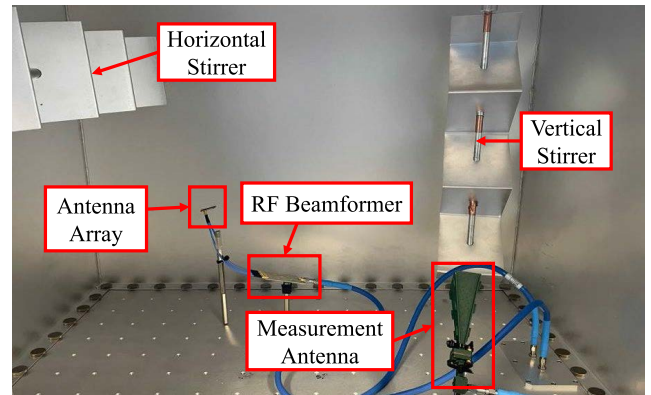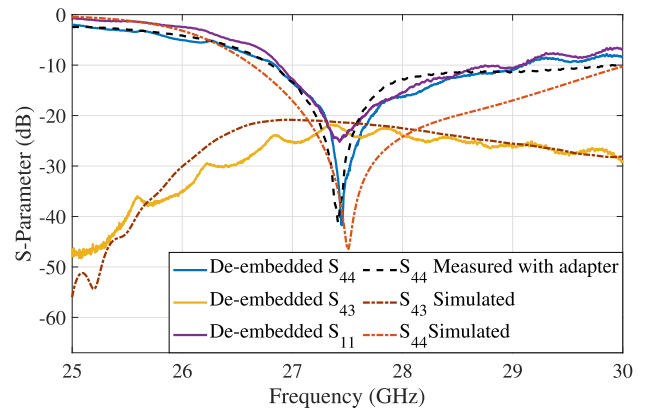
more accurate results as compared to an anechoic chamber when it comes to power-based metrics such as efficiency [15]. Besides that, the reverberation chamber allows for filtering out unwanted radiation sources from other parts of the system and, in this way, evaluate the actual radiation characteristics of the antenna array under test, so overcoming an intrinsic limitation of anechoic chambers [17].

The measured and simulated S-parameter results are shown in Fig. 8. To improve readability, only the S-parameters relevant to the central antenna elements have been plotted. In spite of the narrower bandwidth (with respect to the return-loss level of 10 dB), the measured reflection coefficient is in good agreement with the simulated one. Please note that the S-parameters have been evaluated after de-embedding of the effect of the passive components between the VNA cable and the antenna port using the method described in [16]. The coupling between adjacent elements is below −20 dB.

The radiation pattern measurement setup is shown in Fig. 5 where the antenna array is placed at the center of a mm-wave anechoic chamber which uses a horn antenna as a probe [6], that can be oriented to measure the co- or cross-polarized component of the radiated electromagnetic field (in cross-polarization in Fig. 5). A spherical scan was performed in the far-field, where the radiation patterns in both the E- and H-plane were measured in co-polarization and
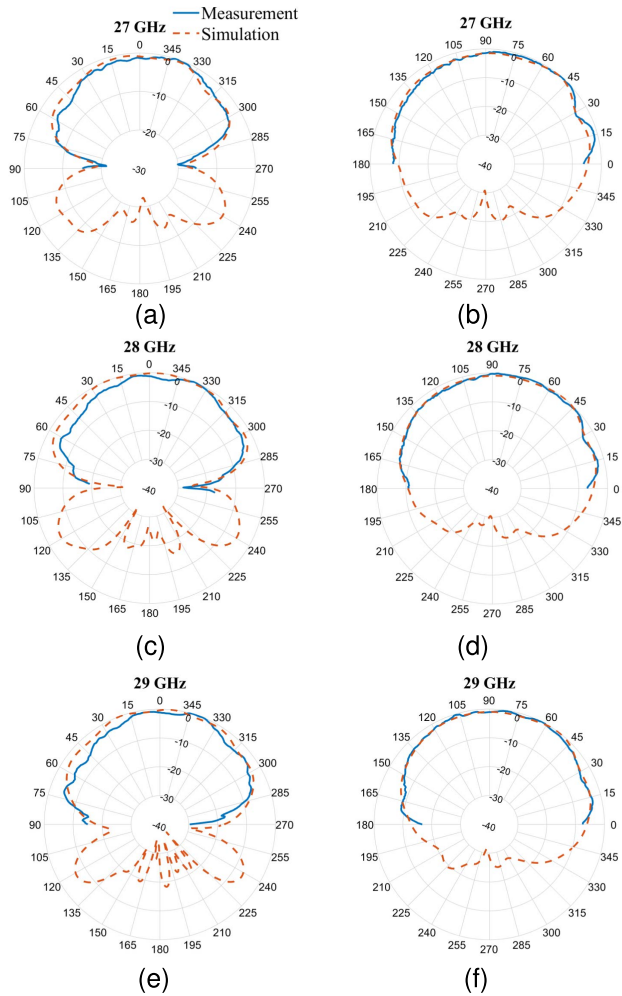
FIGURE 9. Normalized realized gain of the embedded element at (a-b) 27 GHz, at (c-d) 28 GHz and (e-f) at 29 GHz in the $\theta = 90°$-plane on the left column and in the $\phi = 90°$-plane on the right column.

FIGURE 10. (a) Simulated realized gain function of the 1 × 8 linear array while scanning in the $\theta = 90°$-plane at 28 GHz and (b) realized gain measured at 28 GHz.
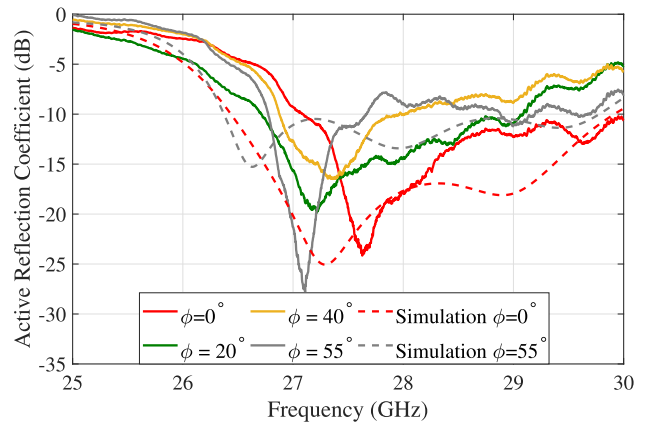
FIGURE 11. Active reflection coefficient while scanning from $\phi = 0°$ to $\phi = 55°$.

cross-polarization. The antenna was placed in the physical center of the chamber. In order to carry out the measurements, 150 mm-long coaxial cables fitted with 1.85 mm to mini-SMP adapters are connected to the antenna array ports. The radiation patterns of the central array element along both $\theta = 90°$ and $\phi = 90°$ planes are shown in Fig. 9 at 27 GHz, 28 GHz and 29 GHz, respectively. The comparison shows a good agreement between simulated and measured results and, in particular, confirms the wide HPBW of the embedded element pattern (approximately 120°). It can also be observed that the embedded radiation pattern is quite stable over the entire frequency range, with a variation of the HPBW below 0.6 dB which assures similar performance as the working frequency changes.

Figs. 10a and 10b illustrate the measured and simulated scanning capabilities of the developed linear array at 28 GHz. The results show that the antenna is able to scan from $\phi = -55°$ to $\phi = 55°$ with a maximal scan loss below 3 dB and a variation with respect to the measurements of 0.2 dB. The results were obtained by evaluating the individual measured embedded element patterns of the various array elements and

by combining the different contributions from each port in post-processing. A peak gain of 13.1 dBi has been simulated with a side lobe level below −10 dB.

For a more extensive characterization of the scanning capabilities of the array antenna, the active reflection coefficient is determined using the de-embedded S-parameters. The results are shown in Fig. 11, only for the scan range from $\phi = 0°$ to

TABLE 2. Uncertainty budget of the efficiency measurement.

Uncertainty Contribution	Standard Uncertainty
Measurement Repeatability	0.1 dB
Radiation Splitter	0.1 dB
Mismatch Cable-Splitter	0.1 dB
Mismatch Splitter	< 0.01 dB
PCB Loss Splitter	0.3 dB
Cable Loss	0.05 dB
Combined Uncertainty (k_p = 1.96)	**0.68 dB**
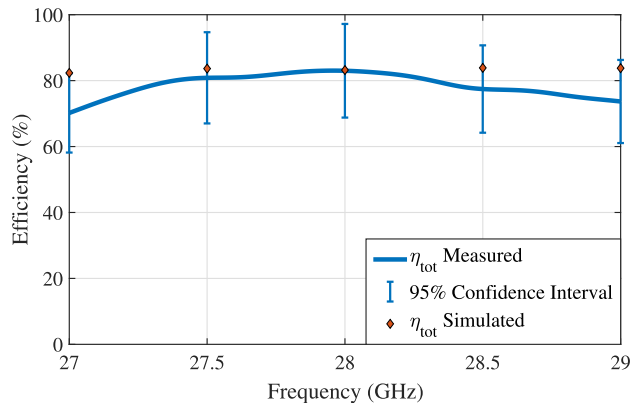
FIGURE 12. Simulated and measured antenna array efficiency when the main beam radiates in end fire in the direction $\phi = 90°$.

$\phi = 55°$ by virtue of the symmetry of the radiating structure. As it can be noticed, the magnitude of the active reflection coefficient is below -7.8 dB over the entire scan range in the considered frequency band.

In order to quantify the losses occurring in the array, antenna-efficiency measurements were performed in a novel mm-wave reverberation chamber. We refer the reader to [17] for an extensive explanation of the operation of this chamber. The antenna efficiency was estimated using the three-antenna method [18]. To this end, two identical standard gain horn (SGH) antennas were used as reference antennas, and three two-antenna measurements were carried out. Since the efficiency of the complete array cannot be estimated out of the efficiency values measured at the individual antenna ports, a Wilkinson splitter was used as an RF beamformer to feed the entire radiating structure at once. The beamformer was de-embedded using the approach in [7]. The setup is shown in Fig. 7. Mode-stirring was performed using two paddle stirrers, stepped using 36° angle spacing, resulting in 100 independent mode-stirring samples. Independence was verified with the *within* correlation approach described in [15], using a threshold of 0.3. The results were averaged over frequency using a running average with a 500 MHz bandwidth.

Due to the stochastic nature of a reverberation chamber, it is common practice to include an uncertainty analysis [15]. The uncertainty contributors and the corresponding standard-uncertainty values are shown in Table 2, which are, in this case, all Type A uncertainties [19]. In this measurement, the RF beamformer quality is the most significant uncertainty contributor, since it has some unwanted radiation, and the PCB losses vary across the different traces. The latter is extracted from the variation across insertion loss

between and is included as 'PCB Loss Splitter' in Table 2. The variation in mismatch between the ports is extracted from the measured reflection coefficients in the same measurements. The measurement repeatability was estimated by carrying out the measurements nine times for different antenna positions and calibrations, and the same approach was used to estimate the uncertainty due to unwanted radiation [20]. The expanded uncertainty was estimated by using the root-sum-square approach as dictated by the CTIA standardized test plan [21], expanded with a coverage factor (k_p) of 1.96. We state that the measurements are in good agreement with the simulations when the simulation results lie within the uncertainty bounds of the measurements, meaning they are statistically not significantly different.

The simulated and measured results for the total efficiency are shown in Fig. 12, the latter reporting the best estimate taken from the mean of the nine measurements. The simulated efficiency values are slightly larger than the measured ones, but always within the 95 % confidence interval of the reverberation chamber. While the efficiency was not measured for different scanning angles, it should be noted that the simulated total efficiency is above 70 % for the entire scan range.

The array design presented in this manuscript is compared to state-of-the-art solutions already proposed in the scientific literature for 5G mobile communication and based on different antenna technologies with end-fire radiation pattern. The benchmarking is performed on the basis of the figures of merit (FoM) reported in Table 3.

In the literature, most of the alternative designs [23], [24], [26] are characterized by a scanning range which is limited to $\pm 40°$ or less. Conversely, the array solution detailed in this research study features measurably wider scanning capabilities which, in turn, can enable a full 3D radio coverage by integration of a reduced number of modules. Furthermore, the proposed array is more compact. Note that the long transmission lines embedded in the physical prototype shown in Fig. 4 are needed only for testing purposes. That being said, such transmission lines in SIW technology are completely shielded from interference and the top and bottom metal layers can be used for accommodating, for example, batteries or other suitable components. Most of the antenna arrays listed in Table 3 are instead considerably larger than the one presented in this work, especially when considering the mobile-device application. Furthermore, the proposed solution is easily scalable to a larger or a smaller number of antenna elements, based on specific requirements.

IV. CONCLUSION
In this paper, a metasurface-based linear array of end-fire like antennas with wide-angle scanning capabilities has been presented. The radiating structure is implemented in SIW technology to enable an easy integration into mainstream PCBs, for use in smartphones or other mobile devices. Furthermore, a metasurface is used to optimize the impedance transformation from the open-ended dielectric-loaded SIW

TABLE 3. Antenna arrays with end-fire radiation pattern proposed in the scientific literature for 5G mobile devices.

Ref.	Antenna technology	Frequency (GHz)	Impedance bandwidth (%)	Peak Gain (dBi)	Volume (mm^3)	Scanning capability	N° antennas
[13]	SIW with metasurfaces	34	42	18.1	N.A.	N.A.	1 × 8
[22]	Magnetoelectric dipole	35	57.6	19	125 × 19.6 × 1.14	N.A.	1 × 16
[23]	SIW horn	27	18.5	9.16	N.A.	-34° ∼ 33°	1 × 4
[24]	Dipole	26	11.3	9.3	63 × 27 × 1.01	-41° ∼ 41°	1 × 4
[25]	SIW loop loaded	28	10	9.51	124.5 × 105 × 3.048	-48° ∼ 48°	1 × 4
[26]	Dipole	3.5 / 28	20.7 / 20.5	4.5 / 9.4	42 × 34 × 0.254	0° ∼ 25°	1 × 4
[27]	Vivaldi	26.5	14	11.2	60 × 28.5 × 0.787	N.A.	1 × 8
This work	**SIW with metasurfaces**	**28**	**10**	**13.1**	**41.5 × 22.6 × 1.5**	**-55° ∼ 55°**	**1 × 8**

to free space. When integrated in a 1 × 8 linear array configuration, the proposed antenna solution can scan from $\phi = -55°$ to $\phi = 55°$ with a scan loss below 3 dB across the frequency range from 27 GHz to 29.5 GHz. The proposed antenna array features a total efficiency level above 70 % and a peak realized gain of 13 dBi at 28 GHz. The realized prototype shows a good agreement between simulated and measured results and a comparison with the state of the art shows how the proposed solution provides a wider scanning range while occupying a smaller volume.

REFERENCES
[1] G. Theis, Z. Song, G. Federico, D. Caratelli, and A. B. Smolders, "A design framework for beamforming integrated circuits operating at mm-Wave frequencies," *IEEE Access*, vol. 9, pp. 62232–62240, 2021, doi: 10.1109/access.2021.3073987.

[2] M. Ikram, K. Sultan, M. F. Lateef, and A. S. M. Alqadami, "A road towards 6G Communication—A review of 5G antennas, arrays, and wearable devices," *Electronics*, vol. 11, no. 1, p. 169, Jan. 2022, doi: 10.3390/electronics11010169.

[3] G. Federico, D. Caratelli, G. Theis, and A. B. Smolders, "A review of antenna array technologies for point-to-point and point-to-multipoint wireless communications at millimeter-wave frequencies," *Int. J. Antennas Propag.*, vol. 2021, pp. 1–18, Apr. 2021, doi: 10.1155/2021/5559765.

[4] M. Bozzi, A. Georgiadis, and K. Wu, "Review of substrate-integrated waveguide circuits and antennas," *IET Microw., Antennas Propag.*, vol. 5, no. 8, pp. 909–920, Jun. 2011, doi: 10.1049/iet-map.2010.0463.

[5] T. Li and Z. N. Chen, "Wideband substrate-integrated waveguide-fed end-fire metasurface antenna array," *IEEE Trans. Antennas Propag.*, vol. 66, no. 12, pp. 7032–7040, Dec. 2018, doi: 10.1109/TAP.2018.2871716.

[6] A. C. F. Reniers, A. Hubrechsen, G. Federico, L. A. Bronckers, and A. B. Smolders, "Spherical mm-wave anechoic chamber for accurate far-field radiation-pattern measurements," in *Proc. Eur. Microw. Week*, 2022.

[7] A. Hubrechsen, A. C. F. Reniers, A. B. Smolders, and L. A. Bronckers, "Chamber-decay time in a mm-Wave reverberation chamber," in *Proc. IEEE Int. Symp. Antennas Propag. USNC-URSI Radio Sci. Meeting (APS/URSI)*, Dec. 2021, pp. 835–836, doi: 10.1109/apsursi47566.2021.9704526.

[8] M. Esquius-Morote, B. Fuchs, J. F. Zürcher, and J. R. Mosig, "A printed transition for matching improvement of SIW horn antennas," *IEEE Trans. Antennas Propag.*, vol. 61, no. 4, pp. 1923–1930, Apr. 2013, doi: 10.1109/TAP.2012.2231923.

[9] Y. Cai, Z.-P. Qian, Y.-S. Zhang, J. Jin, and W.-Q. Cao, "Bandwidth enhancement of SIW horn antenna loaded with air-via perforated dielectric slab," *IEEE Antennas Wireless Propag. Lett.*, vol. 13, pp. 571–574, 2014, doi: 10.1109/LAWP.2014.2312917.

[10] Y. Cao, Y. Cai, L. Wang, Z. Qian, and L. Zhu, "A review of substrate integrated waveguide end-fire antennas," *IEEE Access*, vol. 6, pp. 66243–66253, 2018, doi: 10.1109/ACCESS.2018.2879076.

[11] Y. Cao, Y. Cai, C. Jin, Z. Qian, L. Zhu, and W. Zhang, "Broadband SIW horn antenna loaded with offset double-sided parallel-strip lines," *IEEE Antennas Wireless Propag. Lett.*, vol. 17, no. 9, pp. 1740–1744, Sep. 2018, doi: 10.1109/LAWP.2018.2865587.

[12] K. Yazdandoost and D. Gharpure, "Simple formula for calculation of the resonant frequency of a rectangular microstrip antenna," in *Proc. IEEE 5th Int. Symp. Spread Spectr. Techn. Appl.*, vol. 2, Sep. 1998, pp. 604–605.

[13] J. Tao, X. Li, Y. Li, F. Teng, and H. Wu, "SIW-fed double layer end-fire metasurface antenna array with improved gain," in *Proc. Cross Strait Quad-Regional Radio Sci. Wireless Technol. Conf. (CSQRWC)*, 2019, pp. 1–3, doi: 10.1109/CSQRWC.2019.8799107.

[14] G. Yang and S. Zhang, "Dual polarized wide-angle scanning phased array antenna for 5G communication system," *IEEE Trans. Antennas Propag.*, early access, Jan. 13, 2022, doi: 10.1109/tap.2022.3141188.

[15] A. Hubrechsen, K. A. Remley, and S. Catteau, "Reverberation chamber metrology for wireless Internet of Things devices: Flexibility in form factor, rigor in test," *IEEE Microw. Mag.*, vol. 23, no. 2, pp. 75–85, Feb. 2022, doi: 10.1109/mmm.2021.3125464.

[16] V. Issakov, L. Maurer, M. Wojnowski, and A. Thiede, "Extension of Thru de-embedding technique for asymmetrical and differential devices," *IET Circuits, Devices Syst.*, vol. 3, no. 2, pp. 91–98, Apr. 2009, doi: 10.1049/iet-cds.2008.0276.

[17] A. Hubrechsen, S. J. Verwer, R. Ad C. F., L. A. Bronckers, and A. B. Smolders, "Pushing the boundaries of antenna-efficiency measurements towards 6G in a mm-Wave reverberation chamber," in *Proc. IEEE Conf. Antenna Meas. Appl. (CAMA)*, Nov. 2021, pp. 263–265, doi: 10.1109/cama49227.2021.9703514.

[18] C. L. Holloway, H. A. Shah, R. J. Pirkl, W. F. Young, D. A. Hill, and J. Ladbury, "Reverberation chamber techniques for determining the radiation and total efficiency of antennas," *IEEE Trans. Antennas Propag.*, vol. 60, no. 4, pp. 1758–1770, Apr. 2012, doi: 10.1109/TAP.2012.2186263.

[19] Joint Committee for Guides in Metrology. (Sep. 2008). Evaluation of measurement data—Guide to the expression of uncertainty in measurement. Intl. Bureau Weights Measures, Sevres, France [Online]. Available: http://www.bipm.org/en/publications/guides/gum.html

[20] A. Hubrechsen, G. Federico, G. Verwer, A. S. J. Reniers, A. B. Smolders, and L. A. Bronckers, "De-embedding unwanted radiation from phased-array systems in a reverberation chamber," in *Proc. IEEE Int. Symp. Antennas Propag. USNC-URSI Radio Sci. Meeting (APS/URSI)*, Mar. 2022, pp. 623–624.

[21] *Test Plan for Wireless Large-Form-Factor Device Overthe-Air Performance, Version 1.2.1*, CTIA Certification, Washington, DC, USA, Feb. 2019.

[22] J. Yin, Q. Wu, C. Yu, H. Wang, and W. Hong, "Broadband endfire magnetoelectric dipole antenna array using SICL feeding network for 5G millimeter-wave applications," *IEEE Trans. Antennas Propag.*, vol. 67, no. 7, pp. 4895–4900, Jul. 2019, doi: 10.1109/TAP.2019.2916463.

[23] H. Li, Y. Li, L. Chang, W. Sun, X. Qin, and H. Wang, "A wideband dual-polarized endfire antenna array with overlapped apertures and small clearance for 5G millimeter-wave applications," *IEEE Trans. Antennas Propag.*, vol. 69, no. 2, pp. 815–824, Feb. 2021, doi: 10.1109/tap.2020.3016512.

[24] R. Lu, C. Yu, Y. Zhu, and W. Hong, "Compact millimeter-wave endfire dual-polarized antenna array for low-cost multibeam applications," *IEEE Antennas Wireless Propag. Lett.*, vol. 19, no. 12, pp. 2526–2530, Dec. 2020, doi: 10.1109/lawp.2020.3038790.

[25] Y. Zhu and C. Deng, "Millimeter-wave dual-polarized multibeam endfire antenna array with a small ground clearance," *IEEE Trans. Antennas Propag.*, vol. 70, no. 1, pp. 756–761, Jan. 2022, doi: 10.1109/tap.2021.3098545.

[26] J. Lan, Z. Yu, J. Zhou, and W. Hong, "An aperture-sharing array for (3.5, 28) GHz terminals with steerable beam in millimeter-wave band," *IEEE Trans. Antennas Propag.*, vol. 68, no. 5, pp. 4114–4119, May 2020, doi: 10.1109/TAP.2019.2948706.

[27] S. Zhu, H. Liu, and P. Wen, "A new method for achieving miniaturization and gain enhancement of Vivaldi antenna array based on anisotropic metasurface," *IEEE Trans. Antennas Propag.*, vol. 67, no. 3, pp. 1952–1956, Mar. 2019, doi: 10.1109/TAP.2019.2891220.

GABRIELE FEDERICO (Graduate Student Member, IEEE) received the B.Sc. and M.Sc. degrees in telecommunication engineering from the University of Bologna Alma Mater Studiorum, Italy, in 2013 and 2016, respectively, and the P.D.Eng. degree from the Eindhoven University of Technology, in 2018, where he is currently pursuing the Ph.D. degree with the Electromagnetics Group. His research interests include antenna measurements, antenna array design for mm-wave wireless communications, and RF material characterization.

ANOUK HUBRECHSEN (Graduate Student Member, IEEE) received the B.Sc. and M.Sc. degrees in electrical engineering from the Eindhoven University of Technology, Eindhoven, The Netherlands, in 2017 and 2019, respectively, where she is currently pursuing the Ph.D. degree. She was a Guest Researcher with the National Institute of Standards and Technology at Boulder, Boulder, CO, USA, in 2019, where she was involved in reverberation-chamber metrology for the Internet-of-Things applications. She is currently involved in a Project on reverberation-chamber technology for 5G-and-beyond mm-wave applications and she is a Project Leader within AntenneX. She received the Regional and District Zonta Women in Technology Awards, in 2019. From 2020 to 2021, she was the Vice-Chair of IEEE Benelux Women in Engineering.

SEBASTIAAN LAURENS COENEN received the B.Sc. and M.Sc. degrees in electrical engineering from the Eindhoven University of Technology, The Netherlands, in 2018 and 2020, respectively. He is currently working with Altum RF, where he is a RF Design and Characterization Engineer.

AD C. F. RENIERS received the Ph.D. degree in electrical engineering from the Eindhoven University of Technology (TU/e), in 2022. In the past, he worked at TNO on topics like antenna miniaturization, material characterization, and antenna measurement. He has been affiliated with the Electromagnetics Group, TU/e, since 2009. His current research interests include uncertainties in antenna measurements and material characterization in the millimeter wave frequency range.

DIEGO CARATELLI (Senior Member, IEEE) was born in Latina, Italy, in 1975. He received the M.Sc. degree (*summa cum laude*) in applied mathematics, the Laurea (*summa cum laude*) and Ph.D. degrees in electronic engineering from the Sapienza University of Rome, Rome, Italy, in 2000, 2004, and 2013, respectively. From 2005 to 2007, he was a Research Fellow at the Department of Electronic Engineering, Sapienza University of Rome. From 2007 to 2013, he was a Senior Researcher at the International Research Center for Telecommunications and Radar, Delft University of Technology, Delft, The Netherlands. From 2015 to 2019, he was an Associate Professor at the Institute of Cybernetics, Tomsk Polytechnic University, Tomsk, Russia. In 2013, he co-founded The Antenna Company, Eindhoven, The Netherlands, where he is currently as a Chief Technology Officer/Vice-President of Engineering and is responsible for product development, program portfolio management, and technical direction of the Engineering Team. He has been an Associate Professor with the Group of Electromagnetics in Wireless Telecommunications, Eindhoven University of Technology, Eindhoven, since 2020. He has authored or coauthored more than 200 publications in international peer-reviewed journals, book chapters, and conference proceedings. He holds 22 families of patents in antenna-related technologies and advanced computational techniques. His current research interests include the full-wave analysis and design of passive devices and antennas for satellite, wireless, and radar applications, the development of analytically based numerical techniques devoted to the modeling of wave propagation and diffraction processes, the theory of special functions for electromagnetics, the deterministic synthesis of sparse antenna arrays, and the solution of boundary-value problems for partial differential equations of mathematical physics. He is currently a member of the Applied Computational Electromagnetics Society (ACES), the Institution of Engineering and Technology (IET), the International Union of Radio Science (URSI), and the Italian Electromagnetic Society (SIEm). He was a recipient of the Young Antenna Engineer Prize at the 32nd European Space Agency Antenna Workshop and the 2010 Best Paper Award from ACES. He was a co-recipient of the Frost and Sullivan Best Practices Award for technology innovation in advanced antennas for wireless communications, in 2016. He is the Lead Guest Editor of the Special Issue on Advanced Antenna Array Development for mm-Wave Communications of *Hindawi International Journal of Antennas and Propagation*, and the Special Issue on Theory and Applications of Special Functions in Mathematical Physics of *Symmetry* (MDPI).

A. BART SMOLDERS (Senior Member, IEEE) received the Ph.D. degree in electrical engineering from the Eindhoven University of Technology (TU/e), in 1994. He is an expert in smart antenna systems and worked at TNO, THALES ASTRON, and NXP semiconductors. He has been a Professor with the Electromagnetics Group, TU/e, with special interest in smart antenna systems and applications, since 2010. He currently leads several large research projects in the area of integrated antenna systems for 5G/6G wireless communications. Next to his research activities, he is the Dean of the Electrical Engineering Department.

• • •